Q. J. R. Meteorol. Soc. (2000), **126**, pp. 275–297

Response of the stratosphere to interannual variability of tropospheric planetary waves

By A. A. SCAIFE[1]* and I. N. JAMES[2]
[1] *Meteorological Office, UK*
[2] *Reading University, UK*

(Received 25 June 1998; revised 9 April 1999)

SUMMARY

A primitive-equation global model of the middle atmosphere is used to investigate the response of the extratropical stratosphere to different levels of wave forcing from steady perturbations of the geopotential height near the tropopause. The response of the stratosphere is compared to that in quasi-geostrophic beta-plane models used in previous studies.

The primitive-equation model exhibits three flow regimes under perpetual-January conditions: strong westerly, steady flow for small wave-amplitude forcing, strong westerly but unsteady flow for moderate wave-amplitude forcing and oscillations between easterly and westerly flow for large wave-amplitude forcing. The regimes for low and high forcing are analogous to solutions of the simpler Holton–Mass (HM) quasi-geostrophic model. The moderate-forcing regime does not occur in the HM model and it is attributed to instability of the strongly sheared flow generated by planetary waves in the upper stratosphere. We also show how the observed patterns of interannual variability in the winter stratosphere can be explained in terms of these three flow regimes: in the northern hemisphere the flow often enters the high-forcing regime, where variations in conditions in the early-winter flow or quasi-steady upper-tropospheric planetary-wave amplitudes make similar contributions to the interannual variability in the stratospheric circulation. For the southern hemisphere, we suggest that the flow alternates between the low- and moderate-forcing regimes through year-to-year changes in the amplitude of quasi-steady waves near the tropopause. This mechanism produces large enough changes to explain the interannual variability in the southern stratosphere.

KEYWORDS: Interannual variability Planetary wave Stratosphere–mesosphere model

1. INTRODUCTION

The winter stratosphere exhibits a large amount of interannual variability so that even monthly-mean zonal-mean winds show typical year-to-year differences of 10 m s^{-1} or more (Randel 1992). Numerous studies have suggested possible sources of this variability. These can be classified as internal, such as the possible extratropical effects of the quasi-biennial oscillation (e.g. Holton and Tan 1980; Butchart and Austin 1996), or external, such as the effect of the Southern Oscillation on the lower stratosphere (e.g. Van Loon and Labitzke 1987; Hamilton 1993). Rather than trying to explain the source of the variability, we take a different approach and try to reproduce the observed variability in the stratosphere given only the year-to-year variations in quasi-steady planetary-wave amplitudes near the tropopause.

Quasi-steady planetary-wave forcing from the troposphere is sufficient to drive stratospheric oscillations in quasi-geostrophic models of wave/mean-flow interaction in the stratosphere (Holton and Mass 1976). Furthermore, qualitatively different flow regimes occur in the Holton–Mass (HM) model depending on the amplitude of the waves in the lower-stratospheric height field: at low wave forcing the model approaches a steady state, whereas at high wave forcing, above some critical amplitude, a Hopf bifurcation (to periodic solutions) occurs (Yoden 1987a). This state has oscillations in wave amplitude and between easterly and westerly zonal-mean zonal wind at high latitudes (Yoden 1987b). The transitions to easterly winds strongly resemble observed major stratospheric warmings since the wind reversals extend down to the 10 hPa level and below. It is worth noting that a similar bifurcation from steady to oscillating states also occurs in simple models of the equatorial quasi-biennial oscillation (Yoden and

* Corresponding author: Meteorological Office, London Road, Bracknell, Berkshire RG12 2SZ, UK.

Holton 1988). More recently, Pierce and Fairlie (1993) used approximately a decade of satellite analyses of stratospheric winds and temperatures to find evidence for three flow regimes similar to those in the HM model. It is therefore of interest to investigate whether similar transitions occur in a full primitive-equation model as tropospheric wave amplitudes are varied through the observed range.

Perpetual-January experiments with general-circulation models (GCMs) spanning the troposphere and stratosphere (e.g. Pawson *et al.* 1995; Yoden *et al.* 1996) have shown that similar internal variability to the oscillation in the HM model occurs in the form of irregular series of sudden warmings in the more realistic GCM. However, it is difficult to determine from integrations with a full GCM whether this modelled variability arises internally in the stratosphere or is driven by time-varying forcing from the troposphere. Using a 'fixed troposphere' GCM it has recently been shown that stratospheric oscillations similar to those in the HM model do indeed occur in the more realistic models, even without transient forcing from the troposphere (Christiansen 1999). Here, we use a model that is intermediate between a GCM and the HM model. This makes it ideal to bridge the gap between previous model studies: it is based on the primitive equations with a sophisticated radiation scheme and spherical geometry like the GCM, but the tropospheric state is represented by the lower-stratospheric geopotential height as in the HM model, this allows results to be compared to the HM model for the same lower-boundary planetary-wave forcing.

2. Experiments with a stratosphere–mesosphere model

The UK Meteorological Office (UKMO) stratosphere–mesosphere (SM) model is a global primitive-equation model of the middle atmosphere. Rather than as a forecasting tool, the model is used to investigate the response of the stratosphere to prescribed tropospheric conditions. It has a long history and has been used in many studies of the stratosphere from sudden warmings (Butchart *et al.* 1982), to nonlinear waves (O'Neill and Pope 1988) and tracer transport (Fisher *et al.* 1993). It is a 'mechanistic' model with its lower boundary near the tropopause. The atmosphere below is represented by a prescribed geopotential-height field at 100 hPa in these experiments, one grid spacing below the lowest model level. It has already been shown that geopotential height alone is enough to determine much of the forcing of the atmosphere above and to produce impressive simulations of the observed evolution of the stratosphere (Mote *et al.* 1998).

In all the integrations described here, all zonal asymmetry is introduced via the lower-boundary condition. Given that the SM model incorporates spherical geometry, the planetary-wave forcing used here is equivalent to that used in previous studies with the HM model (Holton and Mass 1976; Yoden 1987a,b): the lower-boundary condition on geopotential height at 100 hPa incorporates the zonal-wave forcing:

$$Z = Z_0 \sin(k\lambda) \cos[l\{\phi - (\pi/3)\}], \tag{1}$$

where λ is longitude and ϕ is latitude. These prescribed waves are steady and stationary with a single zonal wave number (k), meridional wave number l which defines the wave forcing amplitude, and no meridional phase shift. Their amplitude is a maximum Z_0 at 60°N, decreasing sinusoidally to zero at 30°N and the north pole ($l = 3$). No zonal waves are applied at latitudes less than 30°N. When referring to the amplitude of the lower-boundary wave forcing we mean Z_0 from hereon. The model is integrated with constant external conditions in our experiments so that all variability has to originate internally. However, it is worth noting that the Eliassen–Palm (EP) flux through the lower boundary of the model is not strictly constant. This is because geopotential height alone is not

sufficient to specify the EP flux and both winds and temperatures are extrapolated down to the lower boundary from the first two model levels. Internal model variability can therefore cause variations in the EP flux entering the model lower boundary and the wave forcing of the SM model and similar mechanistic models is strictly only quasi-steady.

In these experiments the model is run on a $5° \times 5°$ latitude–longitude grid with 32 quasi-horizontal levels equally spaced in log-pressure to give a vertical resolution of about 2 km. A leapfrog integration scheme is used to solve the primitive equations to fourth-order accuracy in the horizontal and second-order accuracy in both the vertical and time. Eighth-order Shapiro filters (Shapiro 1970) are applied in the zonal and meridional directions and Rayleigh friction is applied to the horizontal wind field in the mesosphere. The Rayleigh friction coefficient is the same as used by Holton (1976); varying with height only, it has a small constant value up to 50 km, increasing exponentially with height above this level on an e-folding scale of 4 km. A time-step of 240 seconds was used in all the integrations. The MIDRAD radiation scheme with prescribed climatological, zonally symmetric ozone and carbon dioxide (Shine 1987; Shine and Rickaby 1989) is used to represent radiative processes. Because this is a mechanistic model, a lower-boundary condition on the upwelling flux of solar radiation reflected from the earth's surface and the troposphere is included. The upwelling infrared radiation from the troposphere is calculated by the method described by Shine (1987). It assumes the troposphere emits black-body radiation at the 700 hPa climatological temperature compiled by Oort (1983).

The integrations were all performed under perpetual-January conditions with incoming radiative fluxes and trace gases set to constant climatological values for 31 January. For the initial conditions we use zonally averaged UKMO TIROS* Operational Vertical Sounder (TOVS) analyses (Bailey *et al.* 1993) for 31 January 1986. The zonally symmetric component of the lower-boundary height field was also taken from this analysis and held constant throughout the integrations. These initial data were chosen to provide undisturbed conditions with westerlies throughout the northern hemisphere extratropics. The TOVS analyses only extend up to 1 hPa and above this level the data were smoothly merged with climatological mean winds from the COSPAR† International Reference Atmosphere (CIRA) climatology (Barnett and Corney 1985). The weighting given to the TOVS data decreased linearly with height above 1 hPa, while the weighting given to the CIRA data increased linearly with height to give a complete initial state for the model up to 0.01 hPa.

To ensure that the experiments covered the observed range of planetary-wave amplitudes, UKMO TOVS data were used to calculate the climatological mean amplitude of the quasi-steady wave-1 (zonal wave-number-1) component of the 100 hPa height field as a function of latitude and for each of the years 1979–1996. Figure 1(a) shows the amplitudes for late northern winter; the waves are calculated from the mean geopotential height for 1 January–28 February when most major warmings occur. Figure 1(b) shows similar amplitudes for the corresponding period in southern winter (1 July–31 August). The lighter lines denote one standard deviation from the mean over 1979–1995 and show that typical ranges in the wave amplitude are 75–200 m in the northern hemisphere and 70–170 m in the south. However, the southern hemisphere waves peak near 45°S and at 60°S the range is only 50–130 m. In order to cover the observed range of amplitudes, various wave-1 amplitudes from zero to 300 m were used to force the model. Sensitivity

* Television Infra-Red Observation Satellite.

† Committee on Space Research.

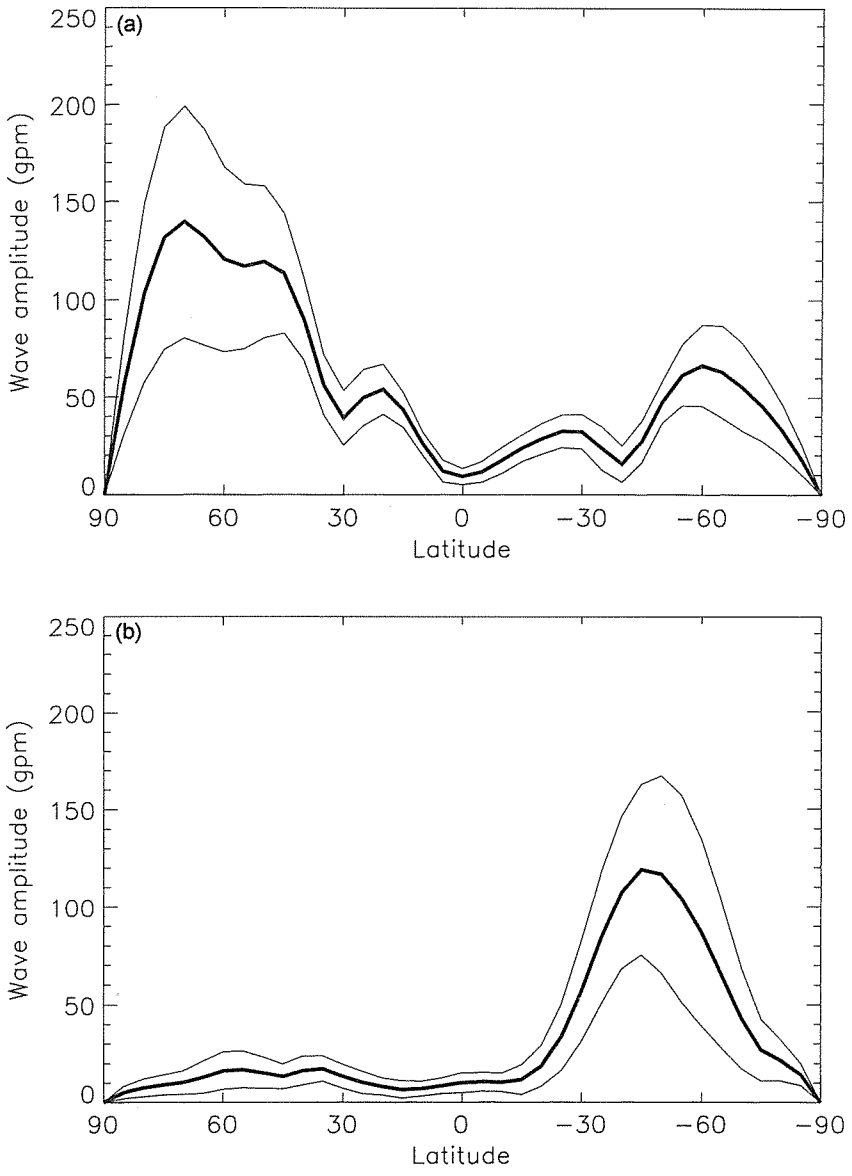

Figure 1. Amplitude of the quasi-steady wave-1 component in UKMO TOVS analyses of the 100 hPa geopotential-height field during late winter. The thick line shows the climatological mean over 1979–1995 and the thin lines indicate one interannual standard deviation for the same averaging period: (a) 1 January–28 February and (b) 1 July–31 August.

to the latitude of maximum wave-amplitude forcing is not tested here since integrations differing by realistic changes in meridional structure enter similar flow regimes to those presented below (Scaife 1998). However, we did investigate the sensitivity to zonal wave number and the integrations with zonal wave-1 forcing were repeated with zonal wave-number-2 and 3 forcing of the same amplitude.

3. THREE FLOW REGIMES

Each of the integrations falls into one of three main types of behaviour or flow regimes which can be identified in time series of the zonal-mean wind. Figure 2 shows the first 120 days of modelled zonal-mean zonal wind at 60°N for an example of each regime. Because the amplitude of planetary waves at the lower boundary determines which regime the model will enter, Figs. 2(a)–(c) are also in order of increasing wave amplitude at 100 hPa.

(*a*) *Small-amplitude forcing, steady regime*

With small-amplitude wave forcing such as 100 m amplitude wave 1, strong steady westerly flow develops and persists as shown in Fig. 2(a).

After some initial transient deceleration in the lower stratosphere in the first few days of the integration, the acceleration to strong westerlies follows a similar evolution to model integrations without any planetary-wave forcing (not shown). The model relaxes towards a state with a cold extratropical stratosphere and a strong polar-night jet with maximum wind speeds of over 100 m s^{-1} near the stratopause. Approximately 100 days are needed to reach this state, as shown for 60°N in Fig. 2(a). In this regime, the structure of the jet is also insensitive to the zonal wave number of the forcing so that with wave-2 forcing and the same wave amplitude of 100 m, the jet is almost identical to that in Fig. 2(a).

This steady regime has only small departures from zonal symmetry in the upper stratosphere. Figure 3(a) shows how the amplitude of zonal wave 1 varies with log-pressure height at 62.5°N in the polar-night jet and after 120 days of integration (the amplitudes are scaled by the square root of density to account for increases with height due to conservative vertical propagation). The amplitude of exactly 100 m at 100 hPa is given by the prescribed waves at the lower boundary and for linear, vertically propagating waves, the scaled amplitude would be constant with height. Between the 100 hPa and 1 hPa levels the wave amplitude first reaches a maximum and then decreases with height to very low values in the upper stratosphere. Also, the phase shift with height shown in Fig. 3(b) is westward but very small through the stratosphere. The overall structure of the wave in this steady state is similar to that noted by Holton and Mass (1976), and although the waves are partially damped it is consistent with reflection of wave activity by the strong westerlies aloft. The strong winds reflect waves back down to interfere with the upward-propagating wave, establishing a standing wave with small vertical phase tilt and a node (essentially zero wave amplitude) in the upper stratosphere. Weak penetration of (presumably evanescent) waves to levels above the wave node can also be seen (but see section 3(b) for a further discussion of this region). These features take several days to become established from what is initially a strong westerly phase tilt with height—a time-scale consistent with the few days required for vertical propagation of Rossby waves through the stratosphere.

Reflection from the model lid (at 1 Pa where the vertical velocity is set to zero) could in principle also occur in the SM model, and this is an alternative explanation of the small vertical phase shifts below. However, this is probably of secondary importance since reflections from the lid would produce a monotonic increase of amplitude with height and would not explain the node in the vertical profile of wave amplitude. The wave node can, however, be explained if the strong winds prevent wave propagation up to this level, as predicted by the Charney–Drazin criterion.

According to linear quasi-geostrophic theory (Charney and Drazin 1961; Dickinson 1968), Rossby waves are only able to propagate into regions where zonal-mean zonal

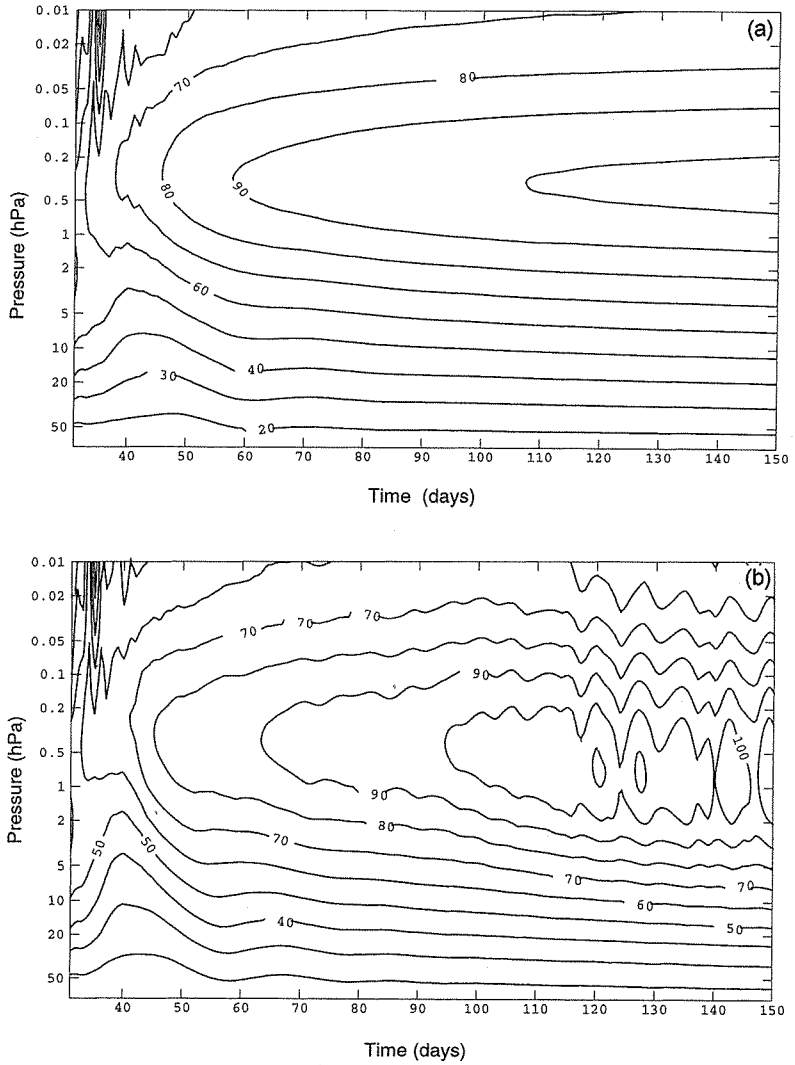

Figure 2. Modelled zonal-mean zonal wind at 62.5°N under perpetual-January conditions. Contour interval is 10 m s^{-1} and shading indicates easterlies. Each plot corresponds to a different flow regime arising from a different amplitude of steady wave-1 forcing in the lower-boundary height field: (a) 100 m, (b) 150 m and (c) 300 m.

winds ($[u]$) are of moderate strength and westerly. By 'moderate' we mean that $[u]$ does not exceed the upper bound in the inequality below:

$$0 < [u] - \frac{\omega}{k} < \frac{[q]_y}{k^2 + l^2 + (f^2/4N^2H^2)}, \tag{2}$$

where

$$[q]_y = \beta - [u]_{yy} - \frac{f^2}{\rho_0}\frac{\partial}{\partial z}\left(\frac{\rho_0}{N^2}\frac{\partial [u]}{\partial z}\right), \tag{3}$$

ω is the intrinsic frequency of the waves (zero for stationary waves), q is quasi-geostrophic potential vorticity, f is the Coriolis parameter, N is the Brunt–Väisälä

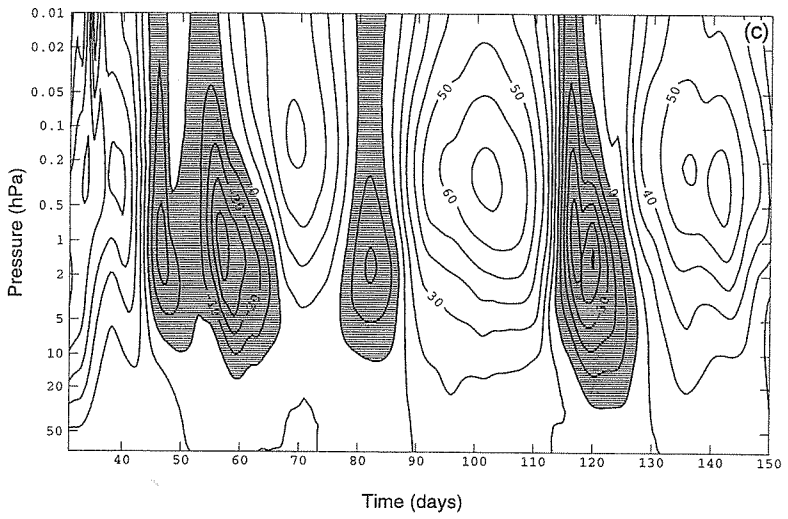

Figure 2. Continued.

frequency, H is scale height, ρ_0 is a reference density which depends only on the height z, β is $\mathrm{d}f/\mathrm{d}y$ and subscripts y and yy denote first and second derivatives with respect to y. Condition (2) implies that higher zonal wave numbers will be restricted to areas of lower zonal wind speed so that, if the standing wave interpretation is correct, forcing with wave 2 will produce a node in the wave amplitude at a lower value of zonal wind than with wave-1 forcing.

This is confirmed by Fig. 3(c) which shows the scaled wave amplitude as a function of height for an integration with 100 m wave-2 forcing. In this case, the node in the vertical profile of wave amplitude occurs at a lower level than for wave-1 forcing. Since the strength of the zonal-mean wind also increases with height in this region, the wave 2 is indeed restricted to lower values of zonal wind speed*.

Condition (2) gives a qualitative guide to the conditions under which planetary waves may propagate when amplitudes are low but it relies on the assumption of a slowly varying background state on the vertical scale of the waves. The maximum value of zonal-mean zonal wind for steady propagating solutions as a function of wave number was calculated from condition (2). Values of the static stability (N^2) and scale height (H) taken from model fields in the upper stratosphere are typically 1.5×10^{-4} s^{-2} and 7.5 km respectively and these give the maximum value of zonal-mean wind for propagation of wave 1 as 45 m s^{-1}, while that for wave 2 is 30 m s^{-1}. These values are comparable to winds in the region where the scaled wave amplitude decreases rapidly with height. Since the model also allows meridional propagation, it might be argued that any discrepancy between the modelled level of reflection and condition (2) is due to waves propagating in from other latitudes. However, $[q]_y$ is close to its maximum value at this point and, according to condition (2), propagation is not allowed into the region surrounding the wave node either. A more likely explanation lies in the variations in zonal flow on the scale of the waves and a mean wind averaged over the large vertical scale of the waves (tens of km) would presumably give closer agreement to (2) and may

* Amplification of the weakly penetrating waves above the wave node gives rise to the large second peak in wave amplitudes seen in the lower mesosphere in Fig. 3(c). For stronger wave forcing this peak in wave amplitudes causes a breakdown in the unsteady flow. This is discussed in section 3(b).

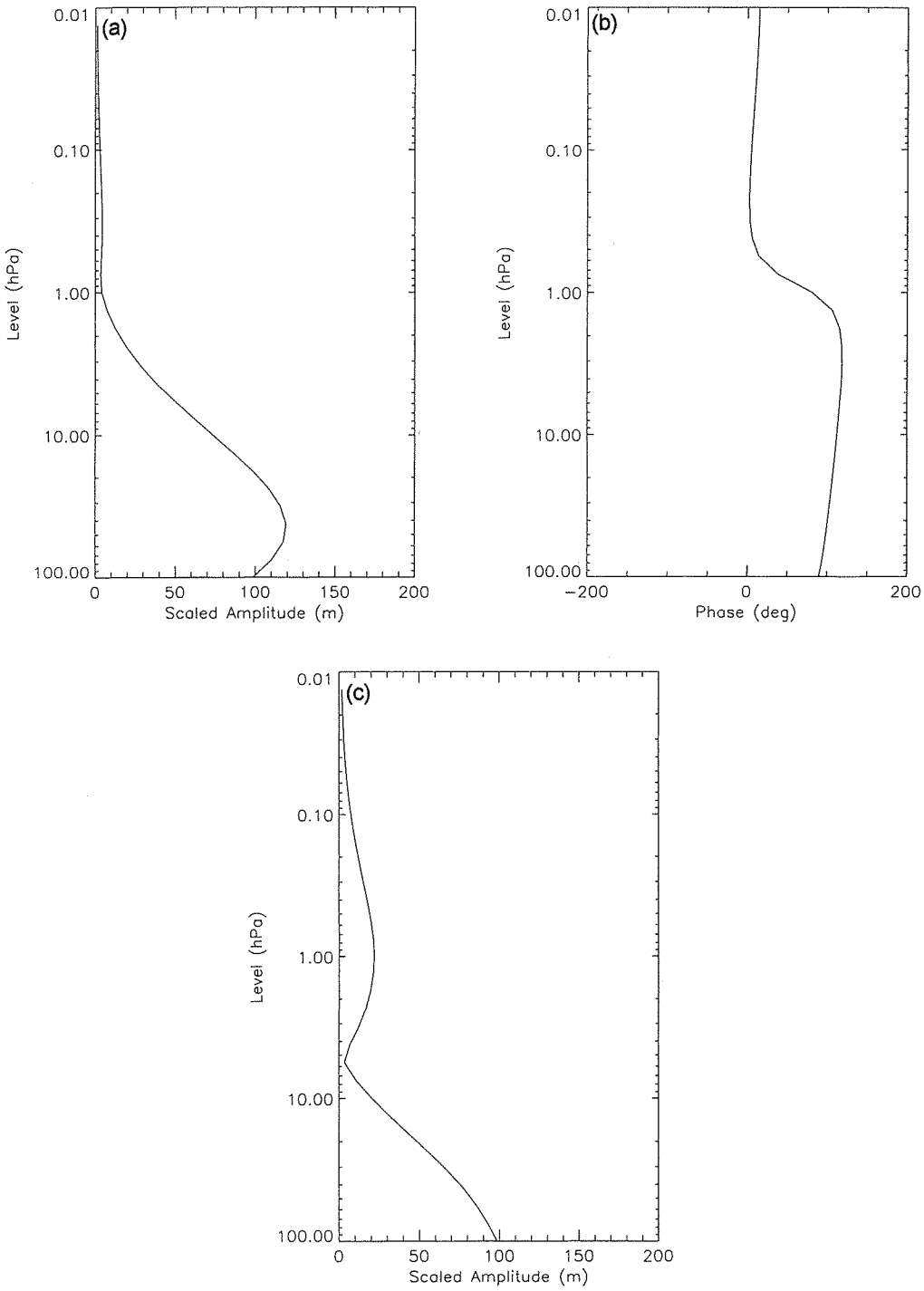

Figure 3. Vertical profiles of the modelled amplitudes (m) and phases (°W) of planetary waves at 62.5°N in the steady regime: (a) amplitude of wave 1 in the integration with 100 m amplitude wave-1 forcing, (b) phase of wave 1 (longitude of ridge) in the same integration, and (c) amplitude of wave 2 in an integration with 100 m amplitude wave-2 forcing. Amplitudes are scaled by the square root of density.

be a more appropriate measure of the background conditions on which propagation is allowed.

Finally, we note that just above the minimum in wave amplitude in these steady states, the waves have negligible vertical phase tilt and there is a small second peak in wave amplitude in the lower mesosphere. This develops when the purely zonal flow at these upper levels is disturbed by the weak vertical penetration of waves beyond the node in amplitude. We now focus on this region as the forcing amplitude is increased.

(*b*) *Moderate forcing, unsteady regime*

With moderate wave forcing amplitude, above a critical value of between 125 and 135 geopotential metres at the lower boundary, a transition to unsteady flow occurs as shown in Fig. 2(b).

This regime is characterized by a quasi-periodic oscillation in zonal-mean wind with a period of about one week and maximum amplitude of approximately 10 m s^{-1} in the core of the polar-night jet. The average period decreases with increasing forcing, from 6 days with 150 m amplitude wave-1 forcing to 4 days when the forcing amplitude is increased to 200 m.

Although the oscillation is easily identified in a zonal mean, it is far from zonally symmetric and the amplitude of planetary waves fluctuates with the same period. Figure 4(a) shows pulses in the amplitude of the zonal wave-number-1 component of the height field at 1 hPa for a few periods of the oscillation. The maximum amplitude occurs near 60°N. Nonlinear effects also play a role since pulses in higher zonal harmonics are found with the same frequency as the pulses in wave 1 in the upper stratosphere, despite the purely zonal-wave-1 forcing of the model at its lower boundary. Figure 4(b) shows the oscillation in the amplitude of zonal wave 2. Note that the maximum in wave 2 occurs at lower latitudes than the maximum in wave 1.

A more detailed view of the longitudinal structure of the oscillation is gained by examining the distribution of Ertel's potential vorticity (EPV) on an isentropic surface. This quantity behaves as a conserved tracer in the absence of friction and radiation (e.g. Hoskins *et al.* 1985) and can be used to trace the motion of air over time-scales for which the flow can be approximated as adiabatic and inviscid. Friction is negligible in the stratosphere and the radiative time-scale is several days at this level (Dickinson 1973), just long enough to examine the oscillation in terms of EPV advection on an isentropic surface. Figure 5 shows a sequence of synoptic maps of the modelled EPV on the 1900 K isentropic surface (in the upper stratosphere) through a single period of the oscillation in this regime. Since the only external source of zonal asymmetry in the integration is the wave-1 forcing at the lower model boundary, it is the phase of these imposed waves at 100 hPa (a positive maximum at 90°W) which determines the location of genesis of the anticyclone near 45°W in Figs. 5(a) and (b). The sequence that follows is similar to that found by Fisher *et al.* (1992) and termed anticyclogenesis. Initially a tongue of low-EPV air is advected northwards and eastwards from the Tropics in the 0–90°W quadrant, shaving off a strip of high potential vorticity from the polar vortex into low latitudes (Fig. 5(a)). The low EPV soon forms the isolated eddy near 20°E in Fig. 5(c) and is advected eastwards before settling 180° east and 20° north of where it was formed. This completes one cycle of the oscillation. This repeating process of travelling eddies feeding into the 90–180° quadrant also reinforces the stationary-wave component of the EPV field at this level and shows the interaction between travelling and stationary waves.

Note from Fig. 2(b) that the oscillation does not begin until the westerly jet (and the horizontal wind shear) is very strong, and that the oscillation has the largest amplitude

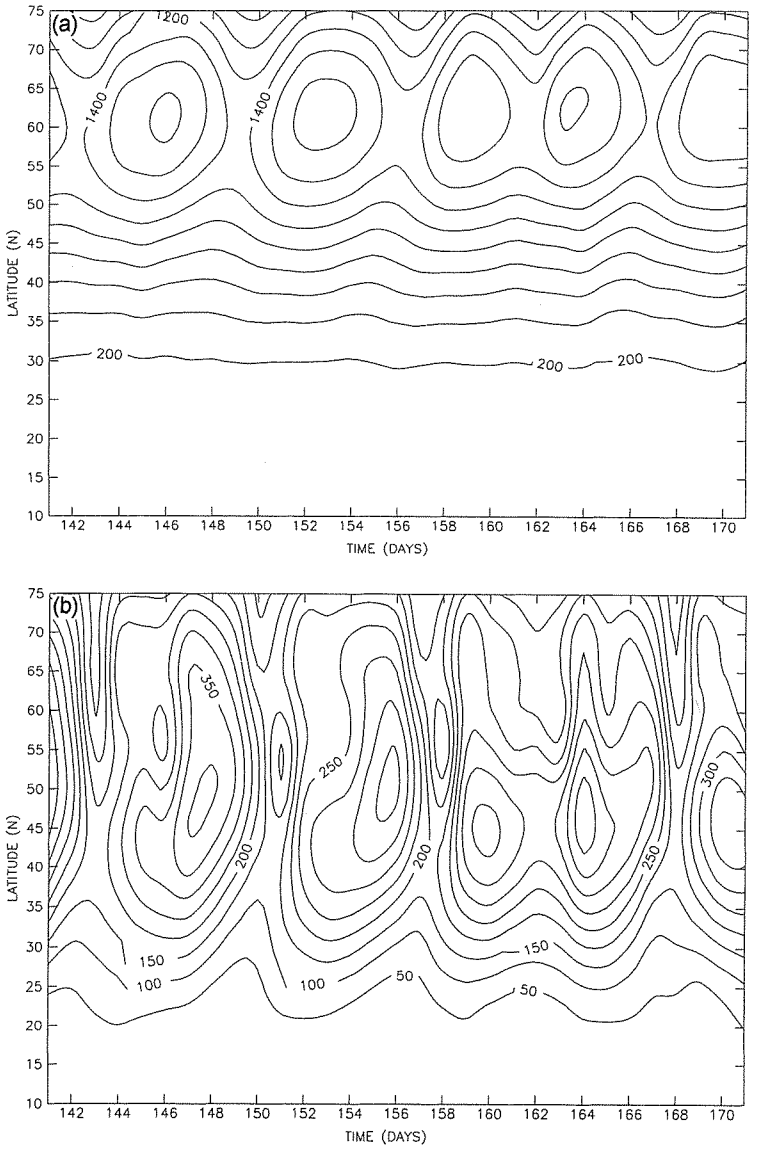

Figure 4. Amplitude (in m) of zonal waves at 1 hPa as a function of latitude and time from an integration with 150 m amplitude wave-1 forcing in the moderate-forcing regime: (a) wave 1 and (b) wave 2.

at the height where the jet is strongest. This occurs irrespective of the zonal wave number used to force the model from the lower boundary (zonal wave 1, 2 or 3), and we suggest that horizontal shear instability may be important in this regime. If the flow contains a sign change of the meridional gradient in the zonal-mean PV field it can be unstable to wave-like perturbations, and this condition holds for the primitive equations if we consider the EPV (James and Hoskins 1985). Figure 5 shows just such a reversed meridional EPV gradient in the 0–90°W quadrant in Fig. 5. A reversed gradient is also apparent in the zonal-mean EPV field (not shown), but instability of the zonal-mean flow is probably not an accurate description of this process since the flow contains strong

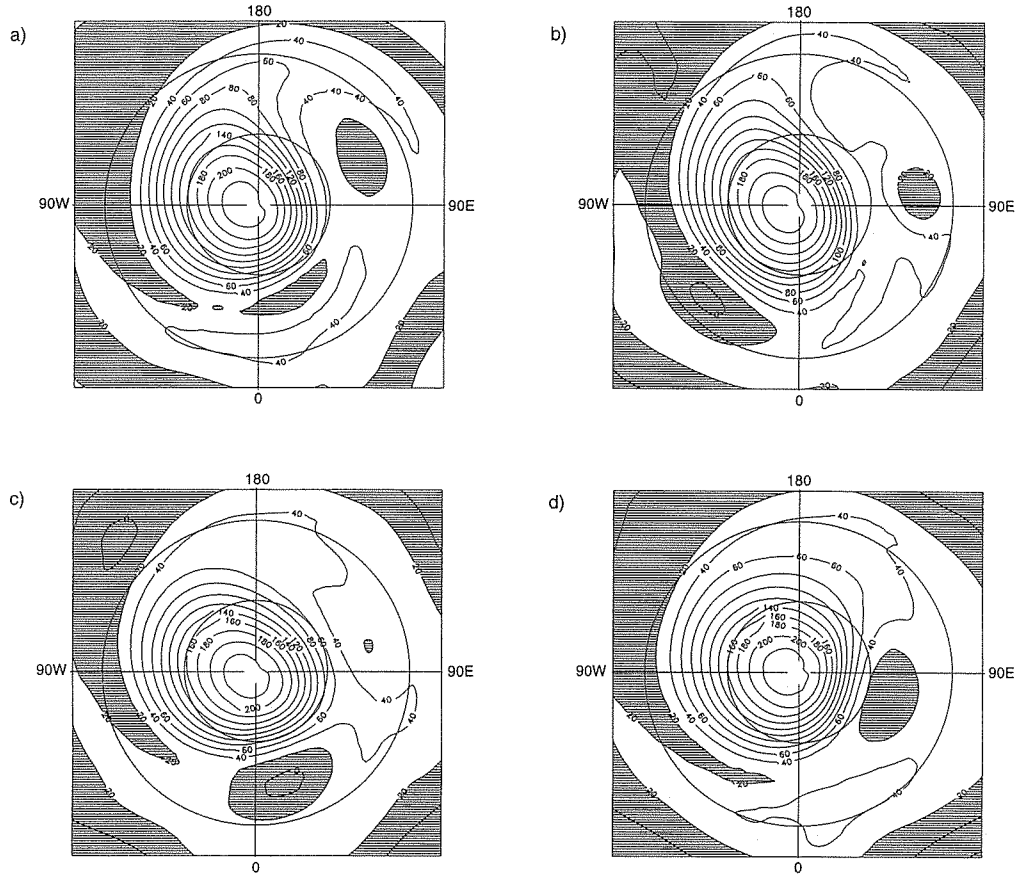

Figure 5. (a)–(c) Modelled Ertel potential vorticity (10^{-4} K $m^2 s^{-1} kg^{-1}$) on the 1900 K isentropic surface at intervals of two days through one period of the oscillation in the moderate-forcing regime with 150 m amplitude wave-1 forcing.

zonal asymmetry. Nevertheless, eastward-travelling eddies have also been produced in a barotropic model of the southern winter stratosphere, with an unstable jet profile similar to that modelled here (Manney *et al.* 1991a). The resulting barotropic waves also show strong similarities to both observed waves (Manney *et al.* 1991b) and those in Fig. 4. Manney's waves show peak wave-2 amplitudes at lower latitudes than the maximum in wave-1 amplitudes as found here.

A second explanation of the moderate-forcing regime involves the nonlinear effects that are significant in this regime. Linear theory neglects wave–wave interactions, but we have already seen interactions between transient and stationary eddies and large pulses in the amplitude of zonal wave 2, despite the lower-boundary forcing containing only zonal wave 1. At least the initial growth of wave 2 is therefore due to nonlinear self-interaction of wave 1 through advection, or perhaps even the action of radiation preferentially damping the ridge of what is initially a wave-1 pattern. The high correlation between pulses in the amplitude of different zonal wave numbers is also consistent with a strong interaction between them. This is made obvious when the oscillation is viewed as the life cycle of an isolated eddy made up of a spectrum of

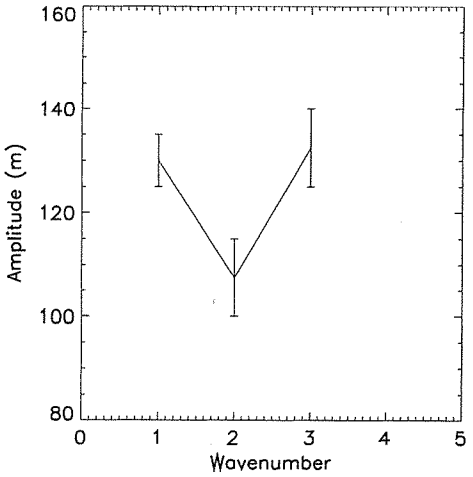

Figure 6. Minimum lower-boundary wave amplitude required to force the transition from the steady (low-forcing) to the unsteady (moderate-forcing) regime within 120 days of integration. Error bars are explained in the text.

waves, since the eddy has both wave-1 and wave-2 components which therefore do not disperse over the eddy lifetime.

Unfortunately, the absence of this moderate-forcing regime from the HM model does not help us to distinguish between the two mechanisms suggested above. Barotropic instability can not occur in the HM model since the imposed meridional structure of the westerly jet in this model is a sine function of latitude, for which $[u]_{yy}$ is always negative, and the poleward gradient of absolute vorticity ($\beta - [u]_{yy}$) is always positive. Since a sign change in this quantity is necessary for instability, the flow is always stable. Similarly, the HM model only represents the interaction of a single zonal mode with the zonal-mean flow and so wave–wave interactions are not allowed either. In view of this it is difficult to decide which mechanism is more important. It seems plausible that shear instability may trigger the formation of eddies but that models able to represent more than just one zonal wave number are needed to resolve the isolated eddies.

Other evidence that barotropic instability may be important comes from the sensitivity of the onset of this regime to the zonal wave number of the lower-boundary forcing. Barotropic models of the southern winter stratosphere with realistic jet structure show that the mode which reaches the largest amplitude has a zonal wave-number-2 structure (Manney *et al.* 1991a). The sensitivity of the onset of the moderate-forcing regime in the SM model shows a similar dependence on zonal wave number: Fig. 6 shows how the critical forcing amplitude for the transition out of the steady state depends on the zonal wave number of the lower-boundary forcing. The error bars indicate the range of uncertainties in this critical amplitude. They were obtained by performing several integrations with the same zonal wave number but different amplitude forcing and then examining which of these exhibit an oscillation after 120 days of integration. The upper amplitude limit defined by the error bar corresponds to the integration with the smallest amplitude forcing sufficient to enter the unsteady regime, while the lower limit on the error bar corresponds to the integration with the maximum height wave amplitude for which the flow remained steady.

The minimum in Fig. 6 indicates that the steady regime is most easily disrupted by wave-2 forcing, since a relatively low-amplitude wave-2 forcing is sufficient to initiate

the oscillation. Providing wave numbers 1 to 3 are able to penetrate up and disturb the upper stratospheric flow, the enhanced sensitivity of this regime to wave-2 forcing may be due to preferential amplification of wave 2 by barotropic instability as found by Manney *et al.* (1991a,b).

(c) *Large-amplitude forcing, major warming regime*

When subjected to large-amplitude wave forcing (e.g. 300 m amplitude wave 1) the model undergoes a series of zonal-mean wind reversals as shown in Fig. 2(c). The wind near 60°N oscillates between westerlies and easterlies and a large sudden increase in the polar temperatures accompanies each reversal to easterlies. This behaviour is very similar to that observed during major sudden warmings, with a positive meridional temperature gradient between 60°N and the pole and easterly zonal-mean wind at (10 hPa, 60°N).

Figure 7(a) shows the amplitude of wave 1 in the geopotential-height field plotted for comparison with the winds in Fig. 2(c). These two figures show that periods of rapidly decelerating zonal-mean winds coincide with large pulses in the amplitude of wave number 1 as expected for wave–mean flow interactions.

In the lower stratosphere, below 10 hPa, the strong easterlies that accompany each warming descend with time. The maxima in wave amplitude also descend with time in this region, as might be expected if a constant flux of waves is prevented from propagating upwards by the descending easterlies. However, in the upper stratosphere and the mesosphere at 1 hPa and above, the zero wind lines show no evidence of downward propagation and easterlies appear simultaneously throughout the depth of the mesosphere.

Each warming is also accompanied by a large pulse in the amplitude of wave 2 as shown in Fig. 7(b). Note that these wave-2 pulses must be initiated internally since the prescribed wave forcing has a purely zonal-wave-1 structure. As in the moderate-forcing regime, the oscillation in this regime is irregular in amplitude and frequency but becomes more frequent as the forcing amplitude is increased: the average period decreases from 100 days for 200 m wave-1 forcing to 40 days for 300 m amplitude forcing.

The horizontal structure of the flow is also very similar to that in observed sudden warmings. Figure 8(a) shows the EPV on the 850 K isentrope in the mid-stratosphere during a typical observed wave-1 sudden warming.* The potential vorticity was calculated from temperatures and geostrophic winds from the UKMO TOVS data, while the TOVS data were themselves calculated by adding layer thicknesses to geopotential height taken from operational analyses for the troposphere (Bailey *et al.* 1993). Comparing with Fig. 8(b) for one of the modelled warmings in the high-forcing regime, we see that in both observed and modelled warmings, a remnant of the polar vortex (high EPV) is displaced equatorwards by a large anticyclone containing relatively uniform EPV, while a tongue of high EPV wraps around this anticyclone. This structure is often observed during major warmings (Palmer and McIntyre 1983), and the similarity to the modelled EPV distribution in Fig. 8(b) shows that the oscillations generated by the simple steady-height waves in (1) reproduce these features of observed warmings in impressive detail.

Finally, note that the range of forcing amplitudes for the moderate- and high-forcing regimes overlap. With wave-1 forcing of 200 m amplitude, both the high-frequency,

* We use 'wave-1' warming to denote those major warmings where the polar vortex is displaced from the pole, as opposed to 'wave-2' warmings where the vortex splits in two.

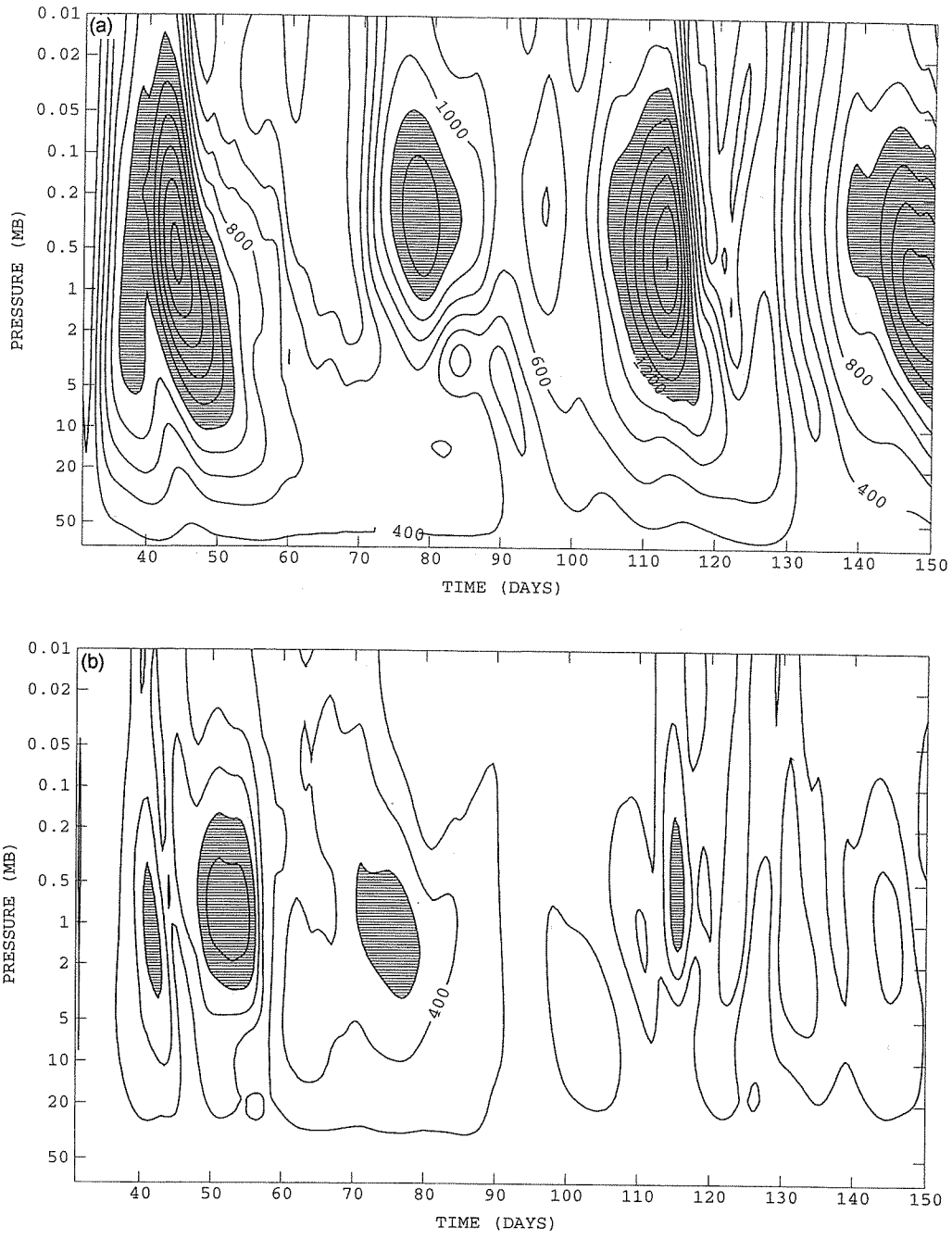

Figure 7. Amplitude (m) of geopotential-height waves at 62.5°N as a function of pressure and time from the high-forcing regime with 300 m wave-1 lower-boundary forcing, contour interval 200 m: (a) zonal wave 1 with shading above 1200 m, and (b) zonal wave 2 with shading above 600 m.

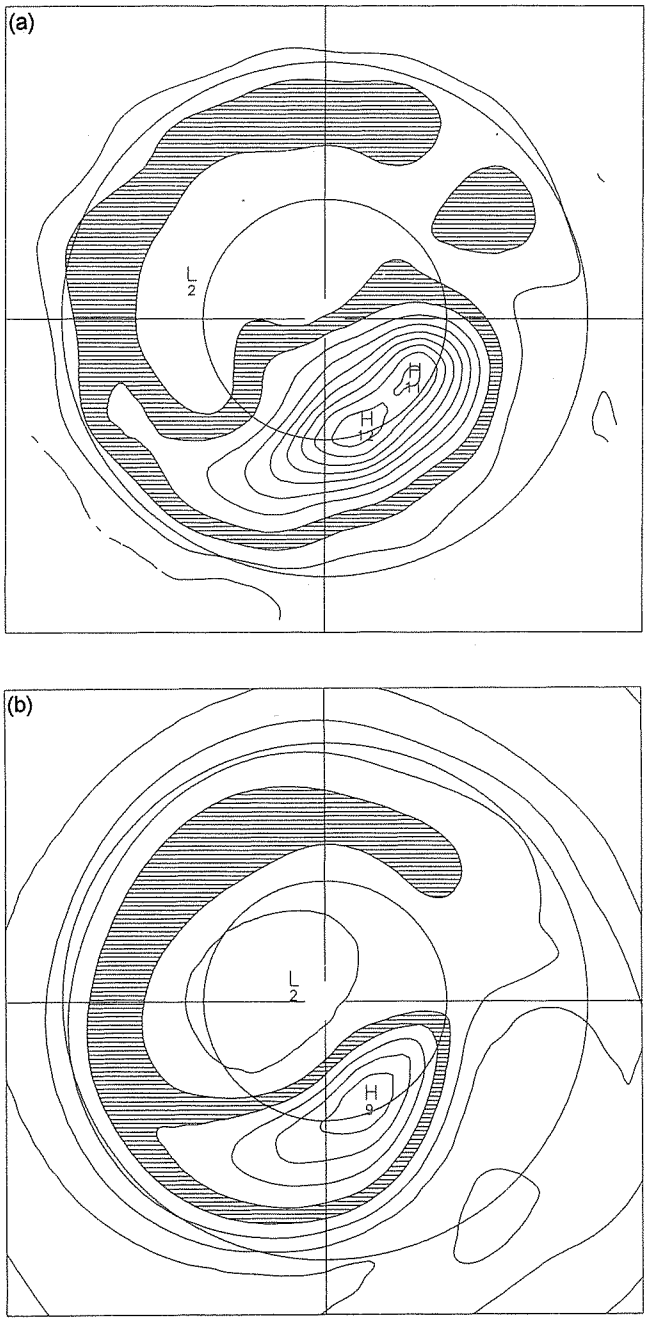

Figure 8. Polar stereographic projection of Ertel's PV (10^{-4} K $m^2s^{-1}kg^{-1}$) on the 850 K isentropic surface during sudden warmings: (a) SSU analyses for 19 January 1987 with shading between 3×10^{-4} and 4×10^{-4} K $m^2s^{-1}kg^{-1}$, and (b) SM model integration in the high-forcing regime with 300 m wave-1 forcing, shaded between 4×10^{-4} and 5×10^{-4} K $m^2s^{-1}kg^{-1}$. Latitude circles are marked at 30° and 60° and the contour interval is 10^{-4} K $m^2s^{-1}kg^{-1}$.

small-amplitude oscillation from the moderate-forcing regime and the sudden warmings from the high-forcing regime are found superimposed in time series of zonal-mean zonal wind. However, we still distinguish the high-frequency oscillation from the longer period sudden warmings since the frequency of the oscillation in the moderate-forcing regime increases with wave forcing amplitude and the long period and large amplitude of the major warmings in the high-forcing regime is never attained. Despite this, the overlap of the two oscillations may well influence details of individual sudden warmings as transient eddies, like those in the moderate-forcing regime, reinforce the stationary-wave component of the flow as we saw in section 3(b).

4. Comparison with the Holton–Mass (HM) model.

The HM model is a quasi-geostrophic beta-plane model of the stratosphere with a Newtonian cooling approximation to radiative processes. Tropospheric planetary waves are introduced into this model via a steady lower-boundary condition on the geopotential height which is the beta-plane equivalent of (1). In this model, although the wave interacts with the zonal-mean flow, neither meridional propagation nor wave–wave interactions are permitted. Given the same lower-boundary forcing of the SM model, we are now in a position to compare previously reported results from the HM model to those from the primitive-equation SM model with its more sophisticated radiation scheme and global domain.

The HM model shows distinct, steady and unsteady flow regimes despite a lack of any imposed transient forcing. The same is true of the SM model, although further experiments with a range of start conditions would be needed to determine whether the multiple stable equilibria found in the HM model (Yoden 1987a) also occur in the SM model used here.

The steady state found in the SM model has a similar vertical structure to certain steady solutions of the HM model since both have a node in the vertical profile of wave amplitude. However, it seems that at least two quite different zonal-mean zonal-wind profiles can support this type of wave amplitude structure in the HM model: a critical line for stationary waves ($[u] = 0$) just above the wave node (Yoden 1987b), or strong westerlies increasing with height as found by Holton and Mass (1976). The steady states described here for the SM model are similar to the latter case since the westerly zonal-mean winds increase with height. We interpret these two possible values of zonal-mean wind at the node in the HM model (zero and strong westerly) qualitatively as the two limits on $[u]$ for propagation of stationary waves given by condition (2).

One difference between the steady states in the SM model and the HM model is that the phase shift with height, although small, is larger in the SM model. This is presumably because some wave activity is either dissipated or leaks to other latitudes through meridional propagation before it can be reflected to interfere with the upward-travelling wave in the SM model.

Both the HM and SM models require some minimum steady wave forcing in order to produce unsteady flow, but the transition is different in the two models and a third 'intermediate' regime occurs in the primitive-equation SM model. The HM model bifurcates directly from a steady regime into the high-forcing regime as the wave forcing is increased; whereas the SM model passes through a regime with a relatively small-amplitude, high-frequency oscillation before entering the high-forcing regime. This moderate-forcing regime may arise through barotropic instability in the SM model, so it seems likely that this difference is at least partly due to the artificial constraint of a

stable meridional jet structure in the HM model. With a more realistic jet, the HM model would presumably show a regime similar to that found in the SM model.

With large-amplitude forcing, both models enter a regime where the flow is punctuated by reversals in the zonal-mean zonal wind, similar to those associated with observed major warmings. In both models, the average time period between these wind reversals decreases with increasing wave forcing. The reversals are simultaneous at levels above the stratopause, but in the lower stratosphere, the maximum in wave amplitude descends with time. The descent is faster in the SM model. Despite this difference, the sudden warmings in the SM model are accompanied by wind reversals that are surprisingly similar to those found in the HM model with the same 300 m wave-1 forcing from the lower boundary. Given this agreement and the fact that the HM model wind reversals are driven by interaction between the planetary wave and the mean flow, we infer that the same basic mechanism drives the major warmings in the more complex SM model.

A further difference between the model solutions is their periodicity, or lack of it: the steady to unsteady transition in the HM model occurs by a Hopf bifurcation, so the transition is from a steady to a perfectly periodic solution (for the range of parameters studied in Yoden 1987a). In contrast, the SM model shows aperiodic oscillations between easterlies and westerlies. This is perhaps not surprising since the SM model represents a wide spectrum of zonal wave numbers and also allows meridional wave propagation, both of which are likely to reduce the reversibility and periodicity of the flow (e.g. Robinson 1988). However, Yoden's periodic solutions were only obtained by numerical methods after many hundreds of days of integration as it takes this amount of time for the solution to become attracted to the periodic state. Long integrations of the SM model would therefore be required to verify that solutions never become periodic. Since the time-scale for attaining a periodic state in even the simpler HM model is much longer than the length of a single winter, it seems that both the occurrence and irregularity in timing of the warmings in perpetual-January integrations of GCMs (e.g. Pawson *et al.* 1995) does not need to be attributed to irregular forcing from the troposphere.

Holton and Mass (1976) found a decrease in the critical amplitude required to enter the high-forcing regime as the forcing was changed from wave 1 to wave 2, and they attributed this to the proportionality between poleward transport of quasi-geostrophic potential vorticity and zonal wave number. In contrast, the critical wave-forcing amplitude to generate easterlies in the SM model increases as the zonal wave number used to force the model is increased from wave 1 to wave 2.

A possible explanation of the different sensitivity of the SM model to zonal wave number is that wave–wave interactions remove the sharp distinction between wave-1 and wave-2 forcing in this model; we have already shown how wave-1 forcing of the SM model from the 100 hPa level generates large-amplitude wave-2 structures in the stratosphere (Figs. 7(a) and (b)). These large wave–wave interactions give the wave-1 forcing experiment with the SM model a significant wave-2 component to the flow and therefore a similarity to the wave-2 forcing experiment with the HM model. In contrast, forcing the SM model with a purely wave-2 pattern at 100 hPa will generate higher, even-numbered waves through nonlinear advection, driving the SM model state away from the purely wave-2 flow in the HM model with the same forcing. It therefore appears that wave–wave interactions may partly explain the different sensitivity of the onset of the sudden warming regime to zonal wave number in the two models. Alternatively, planetary wave 2 is also more easily refracted towards low latitudes than wave 1 and so meridional propagation may also decrease the sensitivity of the SM model to higher wave numbers. Whatever the reason for this difference between the models,

our experiments with the SM model suggest that observed sudden warmings will occur for smaller tropospheric wave-1 amplitudes than wave-2 amplitudes. Significant wave–wave interactions are also likely to occur in observed wave-1 warmings as found in our experiments with the SM model.

5. AN EXPLANATION OF OBSERVED INTERANNUAL VARIABILITY

Some interesting differences are to be found in the year-to-year variations in the winter stratosphere of the northern and southern hemispheres. These differences are not only in the magnitude of the variability but also its distribution over the globe. Figure 9 shows the interannual standard deviation in late-winter mean geopotential heights in the upper stratosphere from UKMO TOVS analyses (Bailey *et al.* 1993). This interannual variability was calculated by taking a time-mean of TOVS analyses over the last two winter months (January to February and July to August) and repeating for each of 17 years from 1979 onwards to give a distribution of winter means. Their standard deviation is plotted as Fig. 9. The northern winter is often punctuated by major warmings during this period, and variations in the timing and occurrence of these warmings is what gives rise to most of the observed interannual variability (Labitzke 1982). The fairly zonal pattern with peak variability near the pole in Fig. 9(a) is a result of the large increase in temperature and geopotential height over the polar cap during major warmings. In contrast, Fig. 9(b) shows that the variability in southern hemisphere July–August mean heights is restricted to a collar of high values in the eastern hemisphere with a minimum near the pole. These differences suggest that different mechanisms generate interannual variability in the two hemispheres.

As noted at the beginning of this paper, the winter stratosphere in the southern hemisphere is subject to smaller-amplitude quasi-steady wave forcing than the north. Given the qualitatively different response to different levels of wave forcing, we suggest that the southern hemisphere winter flow switches between the low and intermediate regimes (Figs. 2(a) and (b)), whereas the northern hemisphere often enters the high-forcing regime (Fig. 2(c)). Observed stationary planetary-wave amplitudes (Fig. 1) are in rough agreement with this hypothesis, although transient wave forcing is probably also important in many observed sudden warmings in the northern hemisphere since Fig. 1(a) shows that quasi-steady wave amplitudes do not often reach the 200 m or so required to enter the high-forcing, sudden warming regime.

The observed interannual variability in the northern winter stratosphere may come from differences in the conditions at the start of the winter period as suggested by Yoden (1990). If this is the case, then a set of 60-day means with random start times from the high-forcing regime shown in Fig. 9(a) should give a modelled standard deviation similar to that observed in the northern hemisphere for January to February. Comparing the observed interannual variability in Fig. 9(a) with the modelled variability in Fig. 10(a) shows that the high-forcing regime does indeed contain variability with a similar spatial distribution to the observed variability. This model estimate of interannual variability is a maximum over the pole, decreasing towards low latitudes. However, the amplitude of the pattern is smaller than observed. Both interannual differences in wave amplitudes in the upper troposphere and interannual variability in the timing of transient pulses of wave activity from the troposphere are also likely to be significant in generating the observed northern hemisphere variability.

A similar model estimate of the southern hemisphere winter variability was made by taking the standard deviation of 60-day means with random start times from the moderate-forcing regime. This gives a pattern qualitatively similar to, but an order of

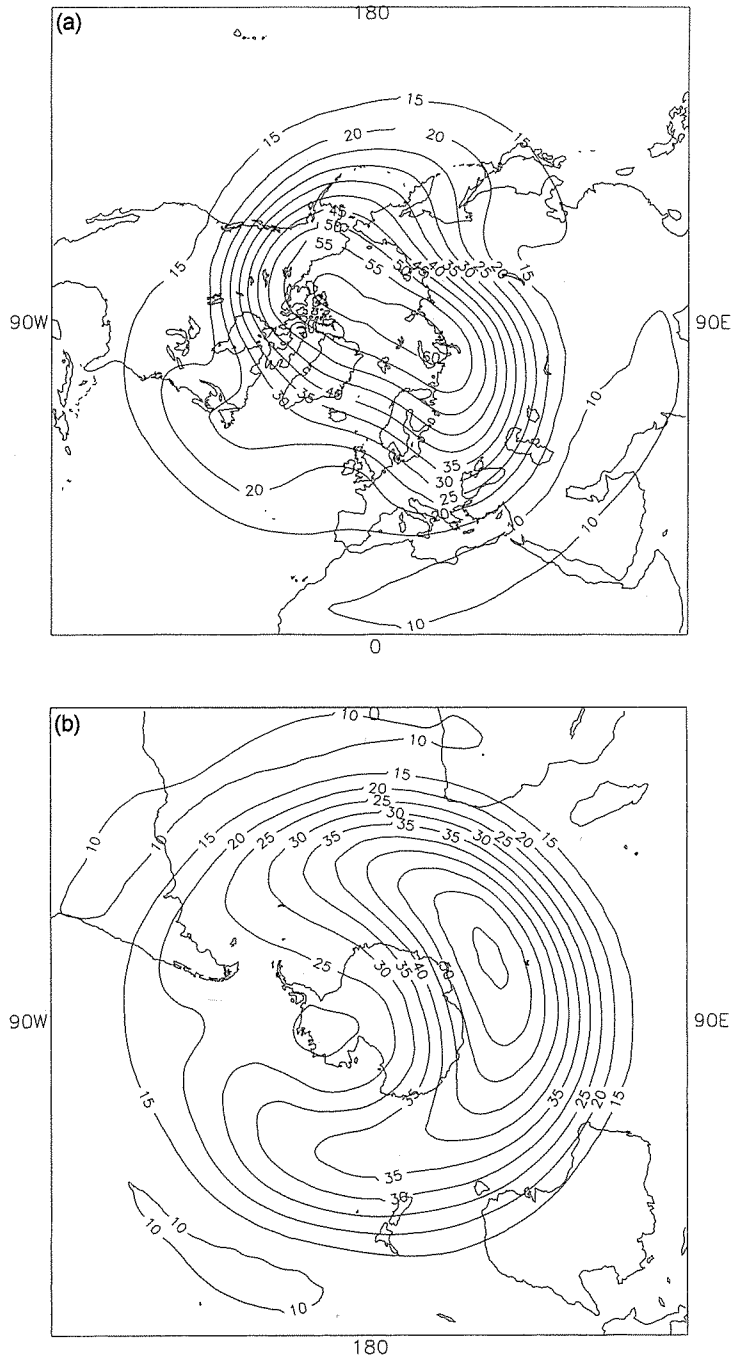

Figure 9. Observed interannual variability in late-winter geopotential height (dam) at 1 hPa from UKMO TOVS analyses for 1979–1995: (a) standard deviation in 1 January–28 February time-means, and (b) standard deviation in 1 July–31 August time-means.

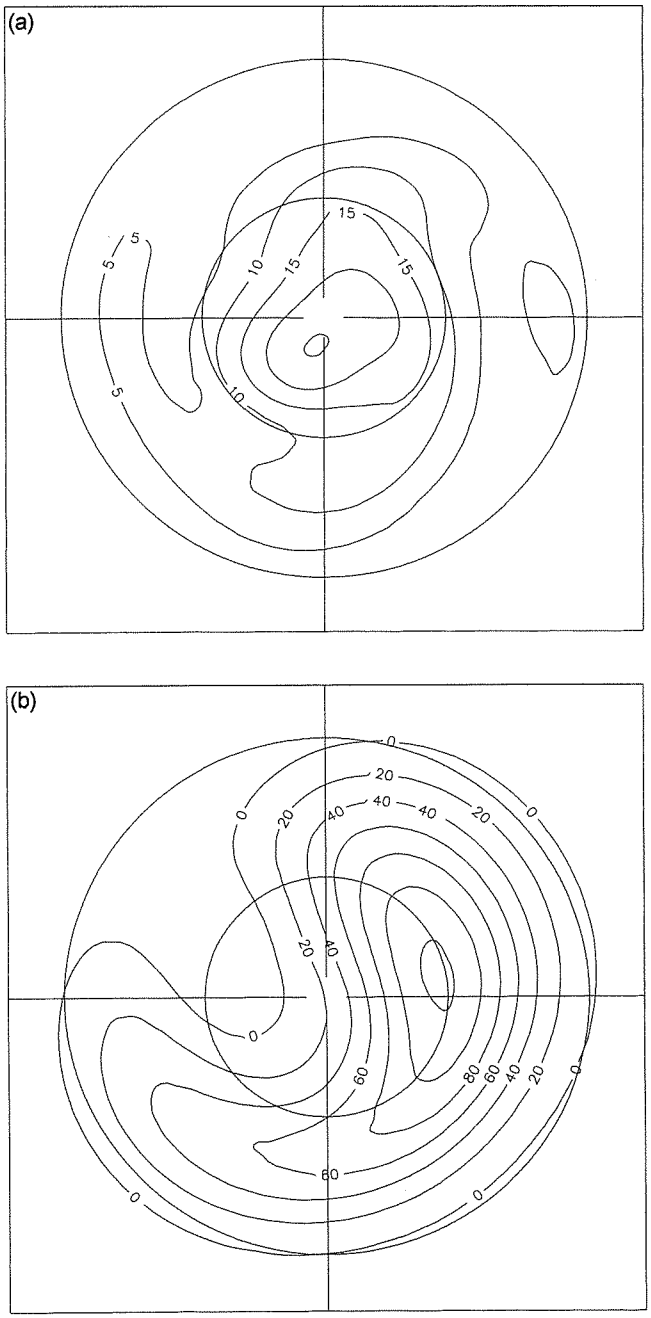

Figure 10. (a) Standard deviation (dam) in 60-day means of the high-forcing regime for comparison with Fig. 9(a), and (b) half the difference (dam) between the time-mean of the steady and moderate-forcing regimes for comparison with Fig. 9(b). Latitude circles are marked at 30° and 60°.

magnitude smaller than the observed variability in Fig. 9(b). In view of this discrepancy, our model of the southern winter is slightly different. Observations of southern winter wave amplitudes (shown in Fig. 1(b)) indicate that the interannual range includes the critical amplitude for the transition from steady to unsteady flow (see Fig. 6). Given this, we postulate that some winters are in the low-forcing regime and others are in the moderate-forcing regime. The simplest estimate of the observed standard deviation is therefore half the difference between time-means from the two regimes. This will be an upper estimate of the variability since it assumes that both regimes occur with equal frequency (a binomial distribution with $p = 0.5$). A frequency distribution weighted in favour of one of the two states would necessarily produce a smaller standard deviation. Figure 10(b) shows the time-mean difference between the low- and moderate-forcing regimes. It has a strikingly similar pattern to the observed variability in Fig. 9(b) with a minimum near the pole and a collar of high values confined to one hemisphere. This collar of increased geopotential height in Fig. 10(b) is the result of averaging over many individual travelling anticyclones of the type shown in Fig. 5 then subtracting off the more zonally symmetric steady state to give the standard deviation. Note that the magnitude of this modelled variability is also adequate to explain the observed variability shown in Fig. 9(b) and is larger than the observed variability, as expected given that the two regimes are assumed to occur with equal frequency in our model estimate.

The three flow regimes from the idealized integrations described here therefore provide a simple model of the interannual variability in the winter stratosphere in terms of the response to variations in the amplitude of quasi-steady, stationary planetary waves from the troposphere.

6. Conclusion

We investigated interannual variability in the winter stratosphere by integrating a mechanistic model under idealized constant external conditions that are based on the range of observed late-winter conditions in the troposphere.

By using the same form of lower-boundary forcing as previous studies which used a simpler, quasi-geostrophic model of wave/mean-flow interaction, it was also possible to compare the two models. The SM model produced some surprisingly similar results to the simple model for the same lower-boundary forcing. In particular, analogues of the steady and high-forcing flow regimes occur in our more sophisticated model. This is despite the large differences between the two models: unlike the HM model, the SM model allows wave–wave interactions and meridional propagation since it is a fully nonlinear 3D model.

A series of aperiodic major warmings characterizes the high-forcing regime. This confirms that realistic major warmings can occur without variations in tropospheric wave amplitudes, and that variability found in the stratosphere of GCMs may not always be attributable to transient forcing from the troposphere. However, the extent to which observed stratospheric transience can be attributed to variations in the tropospheric flow remains an open question. Much longer integrations of the SM model under constant external forcing conditions would also be of interest, to examine more carefully the different modes of internal stratospheric variability found in this model and establish whether these are finally attracted to perfectly periodic solutions as in the HM model.

In addition to the steady and oscillating regimes originally found in the HM model, a third regime was found in the SM model for wave forcing of intermediate strength. We attribute this to instability of the strongly sheared flow on the edge of the polar vortex in regions where the horizontal wind shear is intensified by the stationary-wave component

of the flow. A life cycle of growing and decaying eastward-travelling anticyclones in the upper stratosphere was found.

Finally, we showed how the regimes found in this study offer a simple explanation of the observed interannual variability in the winter stratosphere. As noted by Yoden (1990), the high-forcing regime with its oscillation between easterly and westerly flow in the extratropics resembles the stratosphere during northern winter. This regime shows major stratospheric warmings with periods on a time-scale of months. Providing the observed northern hemisphere flow enters this regime at a different point each winter, it can explain a significant amount of the interannual variability in satellite observations. On the other hand, interannual changes in upper-tropospheric wave amplitudes are also likely to be significant in generating observed northern winter variability in the stratosphere, since changes in wave amplitudes near the tropopause (of similar size to the observed year-to-year variations) proved large enough to drastically alter the frequency of sudden warmings (section 5). It therefore seems likely that both early-winter conditions and year-to-year variations in upper-tropospheric wave amplitudes are important in providing the observed interannual variability in the northern winter stratosphere.

Transitions between the unsteady intermediate regime and the steady low-forcing regime offer a simple explanation of southern winter interannual variability. We suggest that in the southern winter stratosphere, the flow switches between these two states because of interannual variations in the amplitude of winter mean planetary waves near the tropopause. A first guess, assuming that each of the two regimes is equally likely to occur, reproduced the pattern of observed variability in the southern stratosphere remarkably well. However, the variability was larger than observed and an observational study of the winter flow is needed to determine exactly how often the flow is in each of the regimes and to improve on our model estimate of the southern winter interannual variability.

ACKNOWLEDGEMENTS

Many thanks to J. Austin, N. Butchart, A. O'Neill, S. Pawson, R. Swinbank, S. Yoden and the two anonymous reviewers for helpful comments and suggestions.

REFERENCES

Bailey, M. J., O'Neill, A. and Pope, V. D. 1993 Stratospheric analyses produced by the United Kingdom Meteorological Office. *J. Appl. Meteorol.*, **32,** 1472–1483

Barnett, J. J. and Corney, M. 1985 A middle atmosphere temperature reference model from satellite measurements. *Adv. Space Res.*, **5,** 125–134

Butchart, N. and Austin, J. 1996 On the relationship between the quasi-biennial oscillation, total chlorine and the severity of the Antarctic ozone hole. *Q. J. R. Meteorol. Soc.*, **122,** 183–217

Butchart, N., Clough, S. A., Trevelyan, P. J. and Palmer, T. N. 1982 Simulations of an observed stratospheric warming with quasi-geostrophic refractive index as a model diagnostic. *Q. J. R. Meteorol. Soc.*, **108,** 475–502

Christiansen, B. 1999 Stratospheric vacillations in a general circulation model. *J. Atmos. Sci.* (in press)

Dickinson, R. E. 1968 Planetary waves propagating through weak westerly wind wave guides. *J. Atmos. Sci.*, **25,** 984–1002

1973 Method of parametrization for infra-red cooling between the altitudes of 30 and 70 km. *J. Geophys. Res.*, **78,** 4451–4457

Fisher, M., Lawrence, B. and O'Neill, A. 1992 'Idealised simulations of the seasonal evolution of the middle atmosphere for a range of planetary wave amplitudes in the lower stratosphere'. Pp. 33–35 in extended abstracts of 8th Conference on the middle atmosphere. 5–10 January 1992, Atlanta Ga. American Meteorological Society

Fisher, M., O'Neill, A. and Sutton, R. 1993 Rapid descent of mesospheric air into the stratospheric polar vortex. *Geophys. Res. Let.*, **20,** 1267–1270

Hamilton, K. 1993 An examination of observed southern oscillation effects in the northern hemisphere stratosphere. *J. Atmos. Sci.*, **50,** 3468–3473

Holton, J. R. 1976 A semi-spectral numerical model for wave–mean flow interactions in the stratosphere: Applications to sudden stratospheric warmings. *J. Atmos. Sci.*, **33,** 1639–1649

Holton, J. R. and Mass, C. 1976 Stratospheric vacillation cycles. *J. Atmos. Sci.*, **33,** 2218–2225

Holton, J. R. and Tan, H. C. 1980 The influence of the equatorial quasi-biennial oscillation on the global circulation at 50 mb. *J. Atmos. Sci.*, **37,** 2200–2208

Hoskins, B. J., McIntyre, M. E. and Robertson, A. W. 1985 On the use and significance of isentropic potential-vorticity maps. *Q. J. R. Meteorol. Soc.*, **111,** 877–946

James, I. N. and Hoskins, B. J. 1985 Some comparisons of atmospheric internal and boundary baroclinic instability. *Q. J. R. Meteorol. Soc.*, **111,** 2142–2155

Labitzke, K. 1982 Interannual variability of the winter stratosphere in the northern hemisphere. *Mon. Weather Rev.*, **105,** 762–770

Van Loon, H. and Labitzke, K. 1987 The southern oscillation. Part V: The anomalies in the lower stratosphere of the northern hemisphere in winter and a comparison with the quasi-biennial oscillation. *Mon. Weather Rev.*, **115,** 357–369

Manney, G. L., Mechoso, C. R., Elson, L. S. and Farrara, J. D. 1991a Planetary-scale waves in the southern hemisphere winter and early spring stratosphere: Stability analysis. *J. Atmos. Sci.*, **48,** 2509–2523

Manney, G. L., Farrara, J. D. and Mechoso, C. R. 1991b The behaviour of wave 2 in the southern hemisphere stratosphere during late winter and early spring. *J. Atmos. Sci.*, **48,** 976–998

Mote, P., Stott, P. A. and Harwood, S. 1998 Stratospheric flow during two recent winters simulated by a mechanistic model. *Mon. Weather Rev.*, **126,** 1655–1680

O'Neill, A. and Pope, V. D. 1988 Simulations of linear and nonlinear disturbances in the stratosphere. *Q. J. R. Meteorol. Soc.*, **114,** 1063–1110

Oort, A. H. 1983 'Global atmospheric statistics, 1958–1973'. NOAA Technical Report No. 14. Government Printing Office, Washington D.C.

Palmer, T. N. and McIntyre, M. E. 1983 Breaking planetary waves in the stratosphere. *Nature*, **305,** 593–600

Pawson, S., Meyer, A. and Leder, S. 1995 Internal variability in a perpetual-January integration of a troposphere–stratosphere–mesosphere GCM. *Q. J. R. Meteorol. Soc.*, **122,** 369–397

Pierce, R. B. and Fairlie, T. D. A. 1993 Observational evidence of preferred flow regimes in the northern hemisphere winter stratosphere. *J. Atmos. Sci.*, **50,** 1936–1949

Randel, W. J. 1992 'Global atmospheric circulation statistics'. NCAR Technical Note No. 50

Robinson, W. A. 1988 Irreversible wave–mean flow interactions in a mechanistic model of the stratosphere. *J. Atmos. Sci.*, **45,** 3413–3430

Scaife, A. A. 1998 'Interannual variability of the stratosphere'. PhD Thesis, Reading University

Shapiro, R. 1970 Smoothing, filtering, and boundary effects. *Rev. Space Phys.*, **8,** 359–387

Shine, K. 1987 The middle atmosphere in the absence of dynamical heat fluxes. *Q. J. R. Meteorol. Soc.*, **113,** 603–633

Shine, K. and Rickaby, J. A. 1989 'Solar radiative heating due to absorption by ozone'. Pp. 597–600 in Proceedings of Quadrennial IAMAP ozone symposium. 4–13 August 1988, Gottingen. Eds. P. Fabian and R. Bojkov. A Deepak Publishing

Yoden, S. 1987a Bifurcation properties of a stratospheric vacillation model. *Q. J. R. Meteorol. Soc.*, **44,** 1723–1733

1987b Dynamical aspects of stratospheric vacillations in a highly truncated model. *J. Atmos. Sci.*, **44,** 3683–3695

1990 An illustrative model of seasonal and interannual variations of the stratospheric circulation. *J. Atmos. Sci.*, **47,** 1845–1853

Yoden, S. and Holton, J. R. 1988 A new look at equatorial quasi-biennial oscillation models. *J. Atmos. Sci.*, **45,** 2703–2717

Yoden, S., Naito, Y. and Pawson, S. 1996 A further analysis of internal variability in a perpetual January integration of a troposphere–stratosphere–mesosphere GCM. *J. Meteorol. Soc. Jpn*, **74,** 175–188